Estimation of Instrument Spectral Response Functions in Presence of Radiometric Errors

Jihanne El Haouari
TéSA laboratory,
IRIT-ENSEEIHT, CNRS, Univ. Toulouse
Toulouse, France
jihanne.elhaouari@tesa.prd.fr

Jean-Yves Tourneret
TéSA laboratory,
IRIT-ENSEEIHT, CNRS, Univ. Toulouse
Toulouse, France
jean-yves.tourneret@toulouse-inp.fr

Herwig Wendt
IRIT-ENSEEIHT, CNRS, Univ. Toulouse
Toulouse, France
herwig.wendt@irit.fr

Jean-Michel Gaucel
Thales Alenia Space Cannes
Cannes, France
jean-michel.gaucel@thalesaleniaspace.com

Christelle Pittet
Centre National d'Etudes Spatiales
Centre Spatial de Toulouse
Toulouse, France
christelle.pittet@cnes.fr

***Abstract*—High resolution spectrometers, such as the CNES/UKSA MicroCarb instrument, are widely used in remote sensing applications to retrieve atmospheric trace gas concentrations. Potential radiometric errors or errors in the approximation of the Instrument Spectral Response Function (ISRF) can induce significant errors in the determination of these gas concentrations. This paper presents a new strategy for the joint estimation of a spectrometer ISRF and the potential radiometric errors affecting the spectrometer measurements. These radiometric errors are modeled as polynomial functions of the error-free spectrum. An iterative algorithm is then proposed to estimate the coefficients of these polynomials and the spectrometer ISRFs. This algorithm alternates between ISRF estimation steps using the orthogonal matching pursuit algorithm and a radiometric error estimation step using the least squares method.**

***Index Terms*—Instrument spectral response function (ISRF), radiometric errors, sparse representations, OMP.**

I. Introduction

The instrument spectral response function (ISRF) is a key quantity in remote sensing for trace gas retrieval. An imperfect knowledge of the ISRF generally leads to significant errors in the determination of gas concentrations. For the CNES/UKSA MicroCarb mission, relative ISRF approximation errors are expected to be upper bounded by 1%. This bound is not guaranteed by conventional ISRF estimation methods, including those based on the standard Gauss and Super-Gauss models of [1]. Thus, new estimation methods need to be developed, which is the main objective of this paper. The spectrum $S(\lambda_l)$ acquired at wavelength λ_l by the spectrometer is the convolution between a known high-resolution theoretical spectrum S_{th} and the ISRF I_l centered at λ_l [2], [3]:

$$s(\lambda_l) = (s_{\text{th}} * I_l)(\lambda_l) = \int_{\lambda_{\min}}^{\lambda_{\max}} s_{\text{th}}(\lambda_l - u) I_l(u) du. \quad (1)$$

The shape of the ISRF I_l depends on the central wavelength λ_l, which makes the ISRF estimation problem ill-posed, since there is only one measurement per ISRF. To overcome this problem, we assume that the ISRFs do not vary much in an interval around λ_l, which allows all the observations of this interval to be used to estimate the ISRF at λ_l.

In addition to the ill-posed inverse problem (1), radiometric errors can affect the spectrometer measurements at some specific frequencies. This paper introduces a new inverse problem allowing the ISRFs of a spectrometer to be estimated in presence of radiometric errors. In the state-of-the-art, the estimations of the ISRF and the radiometric errors are conducted separately prior to launch [4] through extensive measurement sequences. During in-flight calibration, radiometric errors are mainly considered to be a dark offset and certain gains. Nonlinear radiometric errors are often neglected [5] or approximated using look-up tables (as for the MicroCarb mission).

Goals and contributions. The objective of this work is to solve the ISRF approximation problem in presence of nonlinear radiometric errors affecting the error-free spectrum. The first contribution of this paper is to propose a new model allowing the joint estimation of spectrometer ISRFs and radiometric errors at each wavelength λ_l from the measured spectrum (cf. Section II). The second contribution is an iterative method, described in Section III, which estimates the spectrometer ISRFs and the associated radiometric errors. The ISRFs are approximated using sparse linear combinations of atoms from a known and fixed dictionary and the radiometric errors are estimated using multiple known theoretical spectra. This ISRF estimation method can be used for in-flight calibration. Section IV presents experiments conducted on simulated data from generic models generated by the Centre National d'Etudes Spatiales (CNES) and applied to MicroCarb spectra, which allows the performance of the proposed estimation method to be evaluated. Conclusions are reported in Section V.

II. ISRF approximation and estimation of radiometric errors

A. Radiometric errors

High-resolution atmospheric sounding missions rely on precise on-ground radiometric and spectral calibration [6]. Radio-

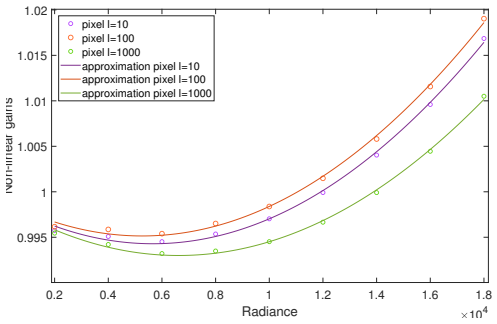

Fig. 1. Examples of non-linear gains for three different pixels with their associated polynomial approximations of degree 2.

metric errors due to the instrument optics are usually estimated from lamp measurements at different radiance levels, during a calibration campaign in a thermal vaccum chamber that simulates the on-orbit environment [7]. These errors are then monitored on orbit using dark, solar and lamp observations. Conversely, this paper introduces a model and its estimation algorithm for estimating ISRFs from a spectrum corrupted by radiometric errors. This section introduces the radiometric errors considered in this work.

Linear gains. The linear gain model is composed of an absolute gain, which is used to convert digital numbers (at a detector pixel level l) to radiances in order to obtain the measured spectra (acquired from solar acquisition), and an inter-pixel relative gain, which is independent of luminance and applies to the useful signal. These two gains are multiplied with the actual spectrum. Note that there is one value of the linear gain per pixel.

Dark current. The dark current is the signal measured by the spectrometer when no light reaches the instrument input. It is an additive error that is added to the spectrum after multiplication by the two linear gains. Note that there is one value of dark current per pixel.

Non-linear gain. A non-linear gain characterizes the presence of non-linearities in the detector. It is defined by a response curve for each pixel as a function of radiance, and is applied to the spectrum with the two kinds of errors described above. This study assumes that for each pixel, the non-linear gain can be modeled accurately by a polynomial. Indeed, from a theoretical point of view, it is well-known that any continuous function defined on an interval can be uniformly approximated by a polynomial function (according to the Stone-Weierstrass approximation theorem [8]). A more practical motivation for using a polynomial model for the non-linearity is that it allows radiometric errors to be approximated with a good accuracy for small polynomial orders. As an illustration, Fig. 1 shows three examples of non-linear gains that can be found in high fluxes and their associated polynomial approximations. Clearly, the non-linear gains can be approximated by second order polynomials with a good accuracy.

B. Problem formulation

Observation model. As seen previously, only one measurement is available for each wavelength λ_l, which leads to a non-identifiable problem. In order to overcome this issue, we make the following assumptions:

- The ISRFs do not vary much within a small window $\mathcal{W}_l = \left\{\lambda_{l-\frac{L}{2}}, ..., \lambda_{l+\frac{L}{2}}\right\}$ of $L+1$ measurements around the wavelength λ_l.
- A sufficiently large number Q of theoretical spectra and their associated measurement vectors associated with the same radiometric errors and the same ISRF are available.

These measured spectra can be obtained during in-flight calibration from some specific scenes (Sun, Moon, etc.) where the theoretical spectrum is rather known. The previous assumptions lead to a vector $\boldsymbol{I}_l \triangleq \left[I_l(-\frac{N}{2}\Delta), ..., I_l(\frac{N}{2}\Delta)\right]^T \in \mathbb{R}^{N+1}$ for each wavelength λ_l, describing the ISRF in the sliding window $\mathcal{W}_l$, where Δ is the ISRF wavelength grid. As explained before, we assume that for each pixel l, the nonlinear gain is a polynomial that is applied to the error-free spectrum with multiplicative and additive errors. These radiometric errors only depend on the instrument used and remain the same for all spectra. The following observation model is thus obtained at each wavelength λ_l:

$$x_{l,q} = f_l\left(s_{l,q}\right) = \sum_{p=0}^{P} d_p^l \left[\boldsymbol{s}_{\text{th},l}^{(q)} \boldsymbol{I}_l\right]^p, \ \forall q = 1, ..., Q, \qquad (2)$$

where f_l is a polynomial of order P, $x_{l,q}$ and $s_{l,q}$ are the lth measurements in presence and absence of radiometric errors respectively, and $\boldsymbol{s}_{\text{th},l}^{(q)} = \left[s_{\text{th}}^{(q)}(\lambda_l - n\Delta)\right]_{-\frac{N}{2} \leq n \leq \frac{N}{2}} \in \mathbb{R}^{N+1}$ where Δ is the wavelength grid. The following notations are then introduced for the $L+1$ measurements of $\mathcal{W}_l$ and the Q theoretical spectra:

- $\boldsymbol{S}_{\text{th},l}^{(q)} \triangleq \left[\boldsymbol{s}_{\text{th},l'}^{(q)}\right]_{l-\frac{L}{2} \leq l' \leq l+\frac{L}{2}} \in \mathbb{R}^{(L+1)\times(N+1)}$ is the matrix containing the qth theoretical spectrum samples,
- $\boldsymbol{S}_l \triangleq \left[s_{l',q}\right]_{l-\frac{L}{2} \leq l' \leq l+\frac{L}{2}, q=1,...,Q} \in \mathbb{R}^{(L+1)\times Q}$ is the matrix of measurements in absence of radiometric errors,
- $\boldsymbol{X}_l \triangleq \left[s_{l',q}\right]_{l-\frac{L}{2} \leq l' \leq l+\frac{L}{2}, q=1,...,Q} \in \mathbb{R}^{(L+1)\times Q}$ is the matrix of measurements in presence of radiometric errors,
- $\boldsymbol{d}_l \in \mathbb{R}^{(P+1)(L+1)}$ is the vector containing the polynomial coefficients of (2) such that $\boldsymbol{d}_l^T \triangleq \left[\boldsymbol{d}_0^l, ..., \boldsymbol{d}_P^l\right]$.

This model can be used to estimate the ISRF $\boldsymbol{I}_l$ and the vector $\boldsymbol{d}_l$ for each wavelength λ_l. Note that for $d_1^l = 1$ and $d_p^l = 0 \ \forall p \in \{0, 2, ..., P\}$, (2) reduces to a discretized version of (1), as described in [9], which can be acceptable for some wavelengths. However, model (1) is not sufficiently accurate for other wavelengths, which motivates this study.

Non-linear inverse problem. The ISRF estimation problem consists in estimating the vector $\boldsymbol{I}_l$ for each wavelength λ_l from the measured spectra in $\boldsymbol{X}_l$. To do so, we introduce the diagonal matrix $\boldsymbol{D}^{(q)}(\boldsymbol{I}_l) = \text{diag}\left(\boldsymbol{S}_l(:, q)\right) \in \mathbb{R}^{(L+1)\times(L+1)}$ containing the qth error-free measurements belonging to the sliding window $\mathcal{W}_l$ (depending on the ISRF) and $\mathbb{1}_{L+1} \in$

$\mathbb{R}^{(L+1)\times(L+1)}$ the $(L+1)\times(L+1)$ identity matrix. Introducing the following matrix

$$\boldsymbol{M}^{(q)}(\boldsymbol{I}_l) = \left[\mathbb{1}_{L+1} \mid \boldsymbol{D}^{(q)}(\boldsymbol{I}_l) \mid ... \mid (\boldsymbol{D}^{(q)}(\boldsymbol{I}_l))^P\right]$$

of size $(L+1)\times(P+1)(L+1)$, this paper proposes to estimate the ISRF $\boldsymbol{I}_l$ and the vector of radiometric error parameters $\boldsymbol{d}_l$ by minimizing the residual errors between $\boldsymbol{X}_l(:,q)$ and its approximation $\boldsymbol{M}^{(q)}(\boldsymbol{I}_l)\boldsymbol{d}_l$, i.e.,

$$\arg\min_{(\boldsymbol{I}_l,\boldsymbol{d}_l)} g_l(\boldsymbol{I}_l,\boldsymbol{d}_l) = \arg\min_{(\boldsymbol{I}_l,\boldsymbol{d}_l)} \sum_{q=1}^{Q} ||\boldsymbol{X}_l(:,q) - \boldsymbol{M}^{(q)}(\boldsymbol{I}_l)\boldsymbol{d}_l||_2^2. \tag{3}$$

III. Iterative estimation method

A. ISRF approximation problem

Sparse representation of ISRFs. Models based on sparse representations and dictionary learning have been extensively used in several applications such as image denoising, classification or restoration [10]–[12]. This paper uses this kind of model for ISRF estimation. The ISRF $\boldsymbol{I}_l$ is modeled as a linear combination of a small number K of atoms from a dictionary $\boldsymbol{\Phi} \in \mathbb{R}^{(N+1)\times N_{\text{dict}}}$ composed of N_{dict} atoms, i.e.,

$$\boldsymbol{I}_l \approx \boldsymbol{I}_l^K = \boldsymbol{\Phi}\boldsymbol{\alpha}_l, \tag{4}$$

where $\boldsymbol{I}_l^K \in \mathbb{R}^{N+1}$ is the approximation of the ISRF $\boldsymbol{I}_l$ obtained using K atoms, and $\boldsymbol{\alpha}_l = (\alpha_{l,1}..., \alpha_{l,N_{\text{dict}}})^T \in \mathbb{R}^{N_{\text{dict}}}$ is a sparse vector with K non-zero coefficients for pixel #l.

Inverse problem without radiometric errors. The convolution between the qth theoretical spectrum and the ISRF $\boldsymbol{I}_l$ can be written using the sparse decomposition (4) leading to:

$$\boldsymbol{S}_l(:,q) \approx \boldsymbol{S}_{\text{th},l}^{(q)}\boldsymbol{I}_l^K = \boldsymbol{\Psi}_l^{(q)}\boldsymbol{\alpha}_l, \tag{5}$$

where $\boldsymbol{S}_l(:,q)$ is the qth column of $\boldsymbol{S}_l$ and new dictionaries are obtained from the theoretical spectra as $\boldsymbol{\Psi}_l^{(q)} \triangleq \boldsymbol{S}_{\text{th},l}^{(q)}\boldsymbol{\Phi} \in \mathbb{R}^{(L+1)\times N_{\text{dict}}}$. The dictionary $\boldsymbol{\Phi}$ and the theoretical spectrum $\boldsymbol{S}_{\text{th},l}^{(q)}$ are assumed to be known and fixed for all $q = 1,..,Q$, so that the new dictionaries $\boldsymbol{\Psi}_l^{(q)}$ are also known. Denote as $\boldsymbol{\Psi}_l \in \mathbb{R}^{Q(L+1)\times N_{\text{dict}}}$ the matrix containing the different dictionaries $\boldsymbol{\Psi}_l^{(q)}$. Estimating the ISRFs from the spectra without radiometric errors concatenated in $\boldsymbol{S}_l$ reduces to a sparse coding problem, i.e., to finding a sparse coefficient vector $\boldsymbol{\alpha}_l$ yielding a good approximation of $\boldsymbol{S}_l$. This problem can be expressed as:

$$\arg\min_{\boldsymbol{\alpha}_l} L(\boldsymbol{\alpha}_l,\mu) = \arg\min_{\boldsymbol{\alpha}_l} ||\text{vec}(\boldsymbol{S}_l) - \boldsymbol{\Psi}_l\boldsymbol{\alpha}_l||_2^2 + \mu||\boldsymbol{\alpha}_l||_0, \tag{6}$$

where the operator vec$(\cdot)$ is introduced to vectorize matrices, $||\cdot||_0$ is the pseudo-norm penalty and μ is an appropriate penalty parameter. Many approximations and heuristics have been proposed to solve this non-convex problem. A widely used family of approaches is based on greedy algorithms, such as Matching Pursuit (MP) or Orthogonal Matching Pursuit (OMP) [13], [14]. This paper will focus on the OMP algorithm that has shown good performance for ISRF approximation [9] and is fast to compute, which is crucial for the targeted application. In what follows, this ISRF estimation method in absence of radiometric errors is referred to as SPIRIT for "SParse representation of Instrument spectral Responses usIng a dicTionary" [9].

B. Estimation and correction of errors for known ISRFs

For a known ISRF, (3) reduces to estimate the vector $\boldsymbol{d}_l$ containing the polynomial coefficients. Since the radiometric errors are the same for different theoretical spectra, this paper proposes to estimate these errors using the least squares problem

$$\arg\min_{\boldsymbol{d}_l} g_l(\boldsymbol{\Phi}\boldsymbol{\alpha}_l, \boldsymbol{d}_l),$$

that has a closed form expression since $g_l(\boldsymbol{\Phi}\boldsymbol{\alpha}_l, \boldsymbol{d}_l)$ is a quadratic function of $\boldsymbol{d}_l$. Once the vector $\boldsymbol{d}_l$ has been determined, the vectors $\boldsymbol{S}_l(l',:)$ (l' row of $\boldsymbol{S}_l$) for $l' = 1, ..., L+1$ can be estimated by searching the roots of the $L+1$ polynomial equations $\boldsymbol{X}_l(l',:) - f_{l'}(\boldsymbol{S}_l(l',:)) = 0 \; \forall l' = 1, ..., L+1$, which results from (2). The solutions of these polynomial equations can be viewed as a way of correcting the radiometric errors.

C. Joint estimation of ISRFs and radiometric errors

Algorithm 1 introduces an iterative algorithm for estimating the ISRFs in presence of radiometric nonlinear errors. This algorithm first performs an initial estimation of the vectors $\boldsymbol{\alpha}_l$ and thus of ISRFs $\boldsymbol{I}_l$ using the SPIRIT algorithm. This algorithm was presented in Section III-A to estimate ISRFs in absence of radiometric errors. In presence of radiometric errors, SPIRIT provides rough ISRF estimations. After initialization, the algorithm iterates three steps until convergence:

- Step 1: estimation of radiometric errors from the previous ISRF estimates and the strategy presented in Section III-B. In practice, the vector $\boldsymbol{d}_l$ is estimated using the MATLAB function *polyfit* to determine the $P+1$ coefficients of the polynomials for the wavelengths belonging to the analysis window,
- Step 2: correction of radiometric errors by determining the zeroes of $\boldsymbol{X}_l(l',:) - f_{l'}[\boldsymbol{S}_l(l',:)]$ (using the MATLAB function *roots*). This operation aims at removing the radiometric errors from the observations $\boldsymbol{X}_l$
- Step 3: re-estimation of the sparse vector $\boldsymbol{\alpha}_l$ from the estimated error-corrected measurements.

This iterative method is an extention of the SPIRIT method that will be referred to as SPIRITUAL for "SParse representation of Instrument spectral Responses usIng a dicTionary assUming polynomiAL radiometric errors".

IV. Numerical experiments

A. Data description

The data used in this paper results from simulations carried out by the CNES for the MicroCarb mission. The instrument considered in this work is a spectrometer with high spectral resolution that has two infrared absorption bands (B2: $1.596-1.618\mu m$ and B3: $2.023-2.051\mu m$) to recover CO_2 absorption lines, and two near-infrared bands (B1:$0.758-0.769\mu m$

Algorithm 1 Iterative ISRF estimation for each window.

Input: Measured spectra $\boldsymbol{X}_l$, Theoretical spectra $\boldsymbol{S}_{\text{th},l}^{(q)}$,
Concatenated dictionaries $\boldsymbol{\Psi}_l$, Desired cardinality K, Number of iterations J
Output: ISRF estimation $\hat{\boldsymbol{I}}_l$, Corrected spectral measurements $\hat{\boldsymbol{S}}_l$

Initialize $\hat{\boldsymbol{d}}_l = [\boldsymbol{0}_{L+1}, \boldsymbol{1}_{L+1}, \boldsymbol{0}_{L+1}, ..., \boldsymbol{0}_{L+1}]^T$;
$\hat{\boldsymbol{\alpha}}_l = \text{OMP}\left(\text{vec}(\boldsymbol{X}_l), \boldsymbol{\Psi}_l, K\right)$;
$\text{vec}(\hat{\boldsymbol{S}}_l) = \boldsymbol{\Psi}_l \hat{\boldsymbol{\alpha}}_l$;
while not convergence **do**
▷ Estimation of radiometric errors using least squares:
  Update: $\hat{\boldsymbol{d}}_l = \arg\min_{\boldsymbol{d}_l} g_l(\boldsymbol{\Phi}\hat{\boldsymbol{\alpha}}, \boldsymbol{d}_l)$;
▷ Error correction by inverting the functions $f_{l'}$ from $\hat{\boldsymbol{d}}_l$ using (2);
  for $l' = 1, ..., L+1$: **do**
    $\hat{\boldsymbol{S}}_l(l', :) = \arg\min_{\hat{\boldsymbol{S}}_l(l',:)} ||\boldsymbol{X}_l(l', :) - f_{l'}[\hat{\boldsymbol{S}}_l(l', :)]||^2$;
  end for
▷ Re-estimation of the sparse vector:
  Update: $\hat{\boldsymbol{\alpha}}_l = \text{OMP}\left(\text{vec}(\hat{\boldsymbol{S}}_l), \boldsymbol{\Psi}_l, K\right)$;
end while
▷ ISRF estimation:
$\hat{\boldsymbol{I}}_l = \boldsymbol{\Phi}\hat{\boldsymbol{\alpha}}_l$
▷ Determination of corrected spectral measurements:
$\hat{\boldsymbol{S}}_l(:, q) = \boldsymbol{S}_{\text{th},l}^{(q)} \hat{\boldsymbol{I}}_l \ \forall \ q = 1, ..., Q$

and B4: $1.264 - 1.282 \mu m$) to measure oxygen concentration. For space reasons, only results for the data from the first band (B1) are reported. The theoretical spectrum is obtained using the radiative transfer software 4A/OP [15]. The ISRFs and observed spectra are constructed using a simulator. For this article, the radiometric errors are simulated as polynomials of degree $P = 3$ and $Q = 41$ theoretical spectra are used for estimating the radiometric errors.

B. Experimental setup

The dictionary is built using $N_{\text{dict}} = 25$ singular vectors associated with the largest singular values of a singular value decomposition (SVD) of 1024 ISRF examples simulated for the chosen band. The size of the observation window is set to $L = 80$ and the number of iterations for the SPIRITUAL algorithm is set to 100. The performance is evaluated in terms of residual error between the actual spectrum $\boldsymbol{S}_l$ and its reconstruction (from the measured spectrum with radiometric errors $\boldsymbol{X}_l$) and normalized absolute error for the ISRF approximation (at a given wavelength), i.e.,

$$\text{E}_l = \sum_{n=1}^{N+1} |\boldsymbol{I}_l(n) - \hat{\boldsymbol{I}}_l(n)| \ / \ \sum_{n=1}^{N+1} \boldsymbol{I}_l(n). \tag{7}$$

C. Results in absence of radiometric errors

In a first part, spectra without radiometric errors are considered. Figure 2 compares the two previously mentioned parametric models of [1] and the model using sparse representation with the OMP algorithm referred to as SPIRIT. As mentioned before, the accuracy required to estimate CO_2 concentrations for the MicroCarb mission requires to know the ISRFs with relative errors less than than 1%. As confirmed in this simulation, the approximation of ISRFs using parametric models [1] does not allow this precision to be obtained, contrary to SPIRIT. The minimum ISRF approximation error is obtained for $K = 4$ atoms used from the dictionary.

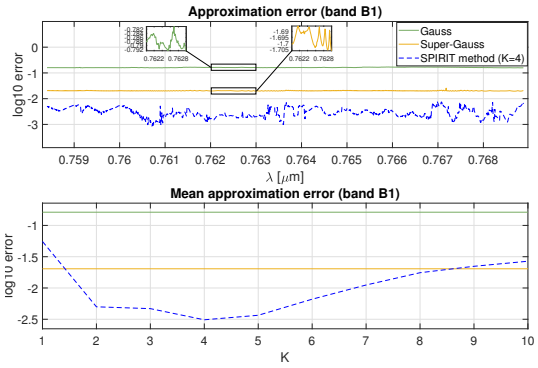

Fig. 2. ISRF approximation errors and mean approximation errors using Gauss, super-Gauss and SPIRIT methods.

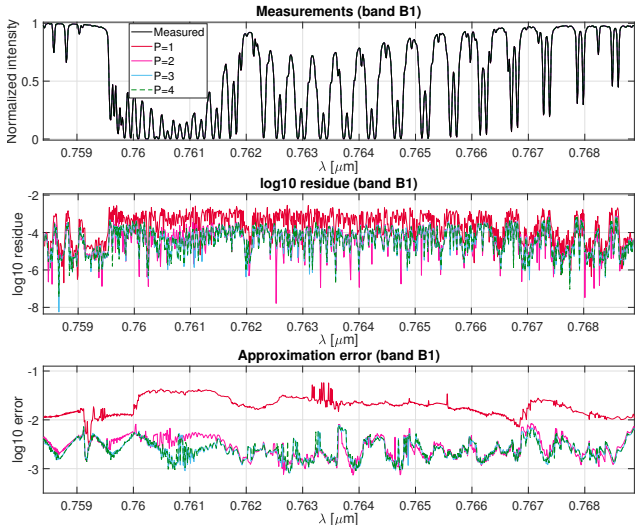

Fig. 3. Spectrum reconstruction for multiple polynomials ($P \in \{1, 2, 3, 4\}$ (top), associated residues (middle) and ISRF approximation errors (bottom).

D. Results in presence of radiometric errors

Estimation of ISRFs and the corresponding spectra. This section applies the SPIRITUAL method with $K = 4$ atoms to estimate radiometric errors, to correct them and to estimate the ISRFs. The degree of the polynomials associated with the radiometric errors has been varied such that $P \in \{1, 2, 3, 4\}$ and the best result in terms of residual error and ISRF approximation error was chosen. Figure 3 illustrates the results for one selected spectrum in term of error-free spectrum reconstruction and ISRF approximation errors for all wavelengths. The best results are obtained for $P \in \{3, 4\}$, where the ISRF approximation errors are below the threshold of 1%.

Examples of estimated ISRFs. Figure 4 shows examples of estimated ISRFs using SPIRITUAL for different polynomial degrees. The approximation errors averaged for all ISRFs in the band $B1$ are also indicated in the figure. We can see that the approximation error decreases as P increases, and that the results obtained for $P = 3$ and $P = 4$ are similar. Finally, as for the mean ISRF approximation error, the value of $P = 3$ is yielding the lowest error.

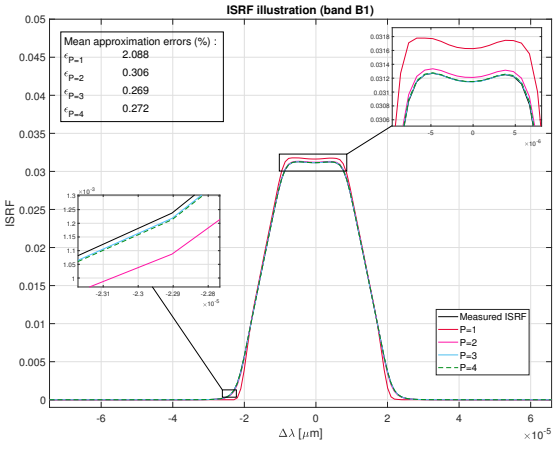

Fig. 4. Examples of ISRF approximations with the corresponding errors for multiple polynomial degrees $P \in \{1, 2, 3, 4\}$.

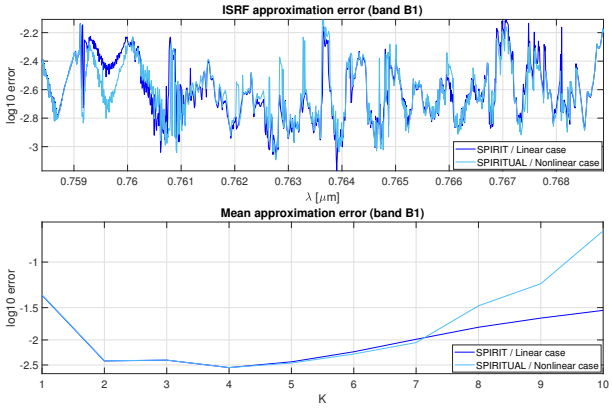

Fig. 5. ISRF approximation errors for SPIRIT and SPIRITUAL with $P = 3$.

E. Comparison between SPIRIT and SPIRITUAL

This section compares the performance of SPIRIT, which assumes no radiometric errors (a best-case scenario) and SPIRITUAL, which accounts for radiometric errors, in terms of ISRF approximation errors and mean approximation errors. Figure 5 shows that the SPIRITUAL method manages to achieve practically the same results as SPIRIT, which is outstanding. It is also interesting to note that relative approximation errors obtained using SPIRITUAL are less than 1%.

V. Conclusion

This paper proposes a new method to estimate the instrument spectral response function (ISRF) of a spectrometer from spectral measurements in presence of radiometric errors. This method, referred to as SPIRITUAL, models radiometric errors using polynomial functions, estimates and corrects these radiometric errors and finally estimates the ISRFs using the corrected measurements. This joint estimation of radiometric errors and ISRF is performed using an iterative process alternating least-squares estimation of radiometric errors, correction of radiometric errors by searching the roots of appropriate polynoms and estimation of sparse vectors using the OMP algorithm. Simulation results suggest that the proposed ISRF estimation method performs almost as well as a method developed for measurements not affected by radiometric errors. Interesting perspectives include the study of the estimation accuracy of the radiometric errors for each pixel of the detector. Future work will also be devoted to analyze the potential interest of machine learning methods and the impact of other degradations such as stray light, additive noise or spectral shifts (that have been neglected in this paper) on ISRF estimation.

References

[1] S. Beirle, J. Lampel, C. Lerot, H. Sihler, and T. Wagner, "Parameterizing the instrumental spectral response function and its changes by a super-Gaussian and its derivatives," *Atmos. Meas. Tech.*, vol. 10, no. 2, pp. 581–598, 2017.

[2] K. Sun, X. Liu, G. Huang, G. González Abad, Z. Cai, K. Chance, and K. Yang, "Deriving the slit functions from OMI solar observations and its implications for ozone-profile retrieval," *Atmos. Meas. Tech.*, vol. 10, no. 10, pp. 3677–3695, 2017.

[3] M. Hamidouche and G. Lichtenberg, "In-flight retrieval of SCIAMACHY instrument spectral response function," *Remote Sens.*, vol. 10, no. 3, pp. 401, 2018.

[4] D. Crisp et al., "The on-orbit performance of the orbiting carbon observatory-2 (OCO-2) instrument and its radiometrically calibrated products," *Atmospheric Measurement Techniques*, vol. 10, no. 1, pp. 59–81, 2017.

[5] M. Zhao, F. Si, Y. Wang, H. Zhou, S. Wang, Y. Jiang, and W. Liu, "First year on-orbit calibration of the chinese environmental trace gas monitoring instrument onboard GaoFen-5," *IEEE Transactions on Geoscience and Remote Sensing*, vol. 58, no. 12, pp. 8531–8540, 2020.

[6] E. Cansot, L. Pistre, M. Castelnau, P. Landiech, L. Georges, Y. Gaeremynck, and P. Bernard, "Microcarb instrument, overview and first results," *Proc. SPIE 12777, Inf. Conf. Space Optics*, vol. 12777, no. 1277734, pp. 1–13, 2022.

[7] R. Rosenberg, S. Maxwell, B. C. Johnson, L. Chapsky, R. A. M. Lee, and R. Pollock, "Preflight radiometric calibration of orbiting carbon observatory 2," *IEEE Transactions on Geoscience and Remote Sensing*, vol. 55, no. 4, pp. 1994–2006, 2017.

[8] M. H. Stone, "The generalized Weierstrass approximation theorem," *Mathematics Magazine*, vol. 21, pp. 167, 1948.

[9] J. El Haouari, J.-Y. Tourneret, H. Wendt, C. Pittet, and J.-M. Gaucel, "Approximation et estimation de réponses spectrales d'instruments," in *Proc. Conf. GRETSI*, Grenoble, France, 2023, pp. p. 85–88.

[10] Z. Zhang, Y. Xu, J. Yang, X. Li, and D. Zhang, "A survey of sparse representation: Algorithms and applications," *IEEE Access*, vol. 3, pp. 490–530, 2015.

[11] K. Schnass and P. Vandergheynst, "Dictionary preconditioning for greedy algorithms," *IEEE Trans. Signal Process.*, vol. 56, no. 5, pp. 1994–2002, 2008.

[12] M. A. T. Figueiredo, R. D. Nowak, and S. J. Wright, "Gradient projection for sparse reconstruction: Application to compressed sensing and other inverse problems," *IEEE J. Sel. Topics Signal Process.*, vol. 1, no. 4, pp. 586–597, 2007.

[13] S. G. Mallat and Z. Zhang, "Matching pursuits with time-frequency dictionaries," *IEEE Trans. Signal Process.*, vol. 41, no. 12, pp. 3397–3415, 1993.

[14] Y. C. Pati, R. Rezaiifar, and P. S. Krishnaprasad, "Orthogonal matching pursuit: recursive function approximation with applications to wavelet decomposition," in *Proc. Asilomar Conf. Signals, Systems and Computers*, Pacific Grove, CA, USA, Nov. 1-3 1993, pp. 40–44.

[15] NOVELTIS, CNES, and LMD, "4A/OP - operational release for 4A - automatized atmospheric absorption atlas," https://4aop.noveltis.fr/references-and-publications.